

# GENERALIZED BEAM MODELS ANALYSIS FOR AEROELASTIC MORPHING APPLICATIONS

Luca Cirrottola<sup>1</sup>, Marco Morandini<sup>2</sup> and Giuseppe Quaranta<sup>3\*</sup>

<sup>1,2,3</sup> Politecnico di Milano, Via La Masa 34, 20156 Milano (Italy)

\*giuseppe.quaranta@polimi.it

**Key words:** Generalized beam theory, Reduced-order modeling, Morphing wing structures

**Abstract.** In the aerospace engineering field, morphing structures refer to mechanical structures capable of adapting their shape in order to improve some vehicle performance. Their analysis requires a computational model detailed enough to represent the internal structural parts which make morphing possible. These are often small with respect to the size of the external structure, so the computational cost of a full 3D finite element model would be high. We restrict our attention to straight, constant cross-section wings and rely on generalized beam theory to develop a computational model capable of analysing the morphing behaviour with a small number of degrees of freedom. We propose an extension of the generalized beam models presented by Morandini et al. (2010). From a singular value analysis of the cross-section finite element model, we derive an additional set of degrees of freedom strictly related to the morphing behaviour, and show the convergence of our projection-based reduced-order structural model to the full order one for some validation cases. The proposed method is applied to the analysis of the FishBAC morphing structure introduced by Woods et al. (2012).

## 1 INTRODUCTION

Morphing aircraft structures, i.e. structures capable of flexible seamless changes of shape, have been re-introduced in the last years for their potential capability of adaptation with a limited weight and reliability penalty [1, 2]. Shape changes on wings include variations in span, twist, camber, and others [1]. Among all possible shape modifications, in this work we focus on camber-morphing, whose application on rotorcraft blades offers significant room for optimizing the performance of the vehicle, included the reduction of vibratory loads and emitted noise [3, 4, 5].

In order to be able to perform a computer simulation of an aeronautical morphing system, the combination of a structural elastic model, an aerodynamic model, and possibly a model of the actuation system is required. The usage of state-of-the-art computational methods (such as finite elements) in every part of this multidisciplinary framework would lead to a complex high-dimensional model, that would require High Performance Computing (HPC) capabilities in order to run the simulations.

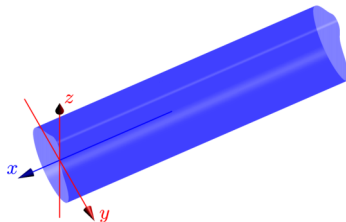


Figure 1: Constant cross-section prismatic solid. Out-of-plane coordinate  $x$ , and in-plane coordinates  $(y, z)$ .

For a computational model that would be competitive (in terms of time and computational resources) with traditional aeronautical design methods, in this work we explore the capabilities of generalized beam models to deal with camber-morphing of straight, slender wings. Several works have focused on generalizing beam models by means of semi-analytical methods providing a detailed characterization of the beam cross-section (summarized in [6]), mostly based on a finite element modeling of the cross-section [7, 6], allowing for composite and anisotropic materials. In [8], it has been shown that classical beam solutions can be obtained without assumptions on the section behaviour, and without any a priori displacement decomposition, once the continuum linear elasticity problem is reformulated as an evolutionary problem along the beam axis [8, 7, 9] and the eigenanalysis of the resulting first order system of linear Ordinary Differential Equations (ODEs) is studied. The six rigid displacements and the six classical polynomial solutions for the beam displacement automatically appear as the solutions generated by the generalized eigenfunctions associated to null eigenvalues. Additional displacement fields (like section warping and additional in-plane deformation) are generated by eigenfunctions associated to non-null eigenvalues, as in the decoupling proposed in [7], and they are exponentially decaying in accordance with de Saint Venant's principle [10, 11].

The aim of this work is to use the formulation presented in [8] to identify a set of solutions clearly related to in-plane deformation, to be used for the derivation of generalized camber-morphing beam models by means of subspace projection of the model equations. This was initiated in [12], where the usage of eigenfunctions related to non-null eigenvalues has been investigated. In this work we investigate an alternative model-projection procedure in order to overcome some of the limitations already encountered in [12].

## 2 SEMI-DISCRETE FORMULATION OF LINEAR ELASTIC MECHANICS

We consider a prismatic three-dimensional elastic solid, with constant cross-section and straight out-of plane  $x$ -axis (fig. 1). In-plane coordinates are labeled as  $\boldsymbol{\xi} \triangleq (y, z)$ .

### 2.1 Virtual work principle

We start from the virtual work principle for a linear elastic continuum [13] in the three-dimensional domain  $\Omega$  occupied by the elastic solid, stating the equality of virtual internal and external work  $\delta\mathcal{L}_i = \delta\mathcal{L}_e$  for every suitable virtual displacement field  $\delta\mathbf{u}$  (a

test function in  $[H_0^1(\Omega)]^3$ ). The virtual external work, considering a cantilever constant cross-section prism of length  $L$  in the interval  $x \in [0, L]$ , can be written as

$$\delta\mathcal{L}_e = \int_{\Omega} \delta\mathbf{u} \cdot \mathbf{f}_{\Omega} \, d\Omega + \int_{\mathcal{S}_L} \delta\mathbf{u} \cdot \mathbf{f}_L \, d\mathcal{A} + \int_{\partial\Omega \setminus \{\mathcal{S}_0 \cup \mathcal{S}_L\}} \delta\mathbf{u} \cdot \boldsymbol{\tau} \, d\Gamma \quad (1)$$

where  $\mathbf{f}_{\Omega}$  represents volume forces,  $\mathbf{f}_L$  represents the surface forces applied on the end section  $\mathcal{S}_L$  (assuming Dirichlet conditions on the root section  $\mathcal{S}_0$ ), and  $\boldsymbol{\tau}$  represents the stress applied on the lateral surface  $\partial\Omega \setminus \{\mathcal{S}_0 \cup \mathcal{S}_L\}$ . The virtual internal work for a linear elastic solid under the small deformation hypothesis is compactly expressed as

$$\delta\mathcal{L}_i = \int_{\Omega} \boldsymbol{\epsilon}(\delta\mathbf{u})^T \mathbf{D} \boldsymbol{\epsilon}(\mathbf{u}) \, d\Omega \quad (2)$$

where the symmetric stress and small strain tensors have been conveniently re-arranged as six-component arrays  $\boldsymbol{\sigma}, \boldsymbol{\epsilon}$ , the latter being related to the displacement field  $\mathbf{u}$  by means of a linear differential operator  $\mathcal{D}$ , with matrix  $\mathbf{D}$  expressing the linear elastic constitutive law

$$\boldsymbol{\epsilon} = \mathcal{D}\mathbf{u} = \begin{bmatrix} \partial/\partial x & 0 & 0 \\ 0 & \partial/\partial y & 0 \\ 0 & 0 & \partial/\partial z \\ \partial/\partial y & \partial/\partial x & 0 \\ \partial/\partial z & 0 & \partial/\partial x \\ 0 & \partial/\partial z & \partial/\partial y \end{bmatrix} \mathbf{u}, \quad \mathbf{D} = \begin{bmatrix} 2\mu + \lambda & \lambda & \lambda & 0 & 0 & 0 \\ \lambda & 2\mu + \lambda & \lambda & 0 & 0 & 0 \\ \lambda & \lambda & 2\mu + \lambda & 0 & 0 & 0 \\ 0 & 0 & 0 & \mu & 0 & 0 \\ 0 & 0 & 0 & 0 & \mu & 0 \\ 0 & 0 & 0 & 0 & 0 & \mu \end{bmatrix} \quad (3)$$

## 2.2 Separation of variables and cross-section discretization

In order to obtain an evolutionary form of the elastic problem along the space direction  $x$ , it is convenient to split the strain tensor  $\boldsymbol{\epsilon}$  into contributions brought by derivatives in the in-plane directions  $\boldsymbol{\xi} \triangleq (y, z) \in \mathcal{S}$ , and by the derivative in the beam axis direction  $x \in [0, L]$

$$\boldsymbol{\epsilon} = \underbrace{\begin{bmatrix} 0 & 0 & 0 \\ 0 & \partial/\partial y & 0 \\ 0 & 0 & \partial/\partial z \\ \partial/\partial y & 0 & 0 \\ \partial/\partial z & 0 & 0 \\ 0 & \partial/\partial z & \partial/\partial y \end{bmatrix}}_{\triangleq \mathcal{D}_{\boldsymbol{\xi}}} \mathbf{u} + \underbrace{\begin{bmatrix} 1 & 0 & 0 \\ 0 & 0 & 0 \\ 0 & 0 & 0 \\ 0 & 1 & 0 \\ 0 & 0 & 1 \\ 0 & 0 & 0 \end{bmatrix}}_{\triangleq \mathbf{S}} \frac{\partial \mathbf{u}}{\partial x} = \mathcal{D}_{\boldsymbol{\xi}} \mathbf{u} + \mathbf{S} \frac{\partial \mathbf{u}}{\partial x} \quad (4)$$

A nodal  $\mathbb{P}_1$  linear finite element discretization for the cross-section domain  $\mathcal{S}$  (which is constant along the  $x$ -axis) is introduced as  $\mathbf{u}(\boldsymbol{\xi}, x) = \mathbf{N}(\boldsymbol{\xi})\mathbf{v}(x)$ . Substitution into the expression of the strain tensor splitting (eq. 4) allows to directly express the strain tensor  $\boldsymbol{\epsilon}$  in terms of the section nodal displacements  $\mathbf{v}(x)$  and their first derivative  $\mathbf{v}'(x) = \frac{d\mathbf{v}}{dx}$  along the beam axis

$$\boldsymbol{\epsilon} = \underbrace{\mathcal{D}_{\boldsymbol{\xi}} \mathbf{N}(\boldsymbol{\xi})}_{\triangleq \mathbf{Z}_{\boldsymbol{\xi}}(\boldsymbol{\xi})} \mathbf{v}(x) + \underbrace{\mathbf{S} \mathbf{N}}_{\triangleq \mathbf{Z}_0} \frac{d\mathbf{v}(x)}{dx} = \mathbf{Z}_{\boldsymbol{\xi}}(\boldsymbol{\xi})\mathbf{v}(x) + \mathbf{Z}_0 \frac{d\mathbf{v}(x)}{dx} \quad (5)$$

Since only matrix  $\mathbf{Z}_\xi(\boldsymbol{\xi})$  retains a dependence from the cross-section coordinates, the last expression allows us to express the volume integral in the virtual internal work (eq. 2) as a multiple integral over the surface  $\mathcal{S}$  and the line  $[0, L]$ , getting

$$\delta\mathcal{L}_i = \int_{\Omega} \boldsymbol{\epsilon}(\delta\mathbf{u})^T \mathbf{D}\boldsymbol{\epsilon}(\mathbf{u}) \, d\Omega = \int_0^L \delta \begin{bmatrix} \mathbf{v} \\ \mathbf{v}' \end{bmatrix}^T \int_{\mathcal{S}} \begin{bmatrix} \mathbf{Z}_\xi^T \mathbf{D}\mathbf{Z}_\xi & \mathbf{Z}_\xi^T \mathbf{D}\mathbf{Z}_0 \\ \mathbf{Z}_0^T \mathbf{D}\mathbf{Z}_\xi & \mathbf{Z}_0^T \mathbf{D}\mathbf{Z}_0 \end{bmatrix} d\mathcal{A} \begin{bmatrix} \mathbf{v} \\ \mathbf{v}' \end{bmatrix} dx \quad (6)$$

Also the virtual external work in eq. 1 can be discretized as

$$\delta\mathcal{L}_e = \int_0^L \delta\mathbf{v}^T \int_{\mathcal{A}} \mathbf{N}^T \mathbf{f}_\Omega \, d\mathcal{A} \, dx + \delta\mathbf{v}^T(L) \int_{\mathcal{S}_L} \mathbf{N}^T \mathbf{f}_L \, d\mathcal{A} + \int_0^L \delta\mathbf{v}^T \int_{\partial\mathcal{A}} \mathbf{N}^T \boldsymbol{\tau} \, d\Gamma \, dx \quad (7)$$

The following matrices can be conveniently defined

$$\mathbf{E} \triangleq \int_{\mathcal{S}} \mathbf{Z}_\xi(\boldsymbol{\xi})^T \mathbf{D}\mathbf{Z}_\xi(\boldsymbol{\xi}) \, d\mathcal{A}, \quad \mathbf{C} \triangleq \int_{\mathcal{S}} \mathbf{Z}_\xi(\boldsymbol{\xi})^T \mathbf{D}\mathbf{Z}_0 \, d\mathcal{A}, \quad \mathbf{M} \triangleq \int_{\mathcal{S}} \mathbf{Z}_0^T \mathbf{D}\mathbf{Z}_0 \, d\mathcal{A} \quad (8)$$

together with the semi-discrete domain and boundary nodal forces

$$\mathbf{F}_\Omega \triangleq \int_{\mathcal{A}} \mathbf{N}^T \mathbf{f}_\Omega \, d\mathcal{A}, \quad \mathbf{F}_L \triangleq \int_{\mathcal{S}_L} \mathbf{N}^T \mathbf{f}_L \, d\mathcal{A}, \quad \mathbf{F}_{\partial\mathcal{A}} \triangleq \int_{\partial\mathcal{A}} \mathbf{N}^T \boldsymbol{\tau} \, d\Gamma \quad (9)$$

so that the virtual work principle can be compactly written in its semi-discrete form as

$$\int_0^L \delta \begin{bmatrix} \mathbf{v} \\ \mathbf{v}' \end{bmatrix}^T \begin{bmatrix} \mathbf{E} & \mathbf{C} \\ \mathbf{C}^T & \mathbf{M} \end{bmatrix} \begin{bmatrix} \mathbf{v} \\ \mathbf{v}' \end{bmatrix} dx = \int_0^L \delta\mathbf{v}^T (\mathbf{F}_\Omega + \mathbf{F}_{\partial\mathcal{A}}) \, dx + \delta\mathbf{v}^T(L) \mathbf{F}_L, \quad (10)$$

$$\forall \delta\mathbf{v} \in [H_0^1([0, L])]^{3n_s}$$

### 3 SUBSPACE PROJECTION AND FULLY DISCRETE FORMULATION

A low-dimensional representation of the unknown  $\mathbf{v}(x) \in H_0^1([0, L])^{3n_s}$  by means of a vector  $\mathbf{k}(x) \in H_0^1([0, L])^{n_r}$ , with  $n_r \ll 3n_s$ , is sought. This is accomplished by finding a matrix  $\mathbf{P} \in \mathbb{R}^{3n_s \times n_r}$  whose columns span a  $n_r$ -dimensional subspace of  $\mathbb{R}^{3n_s}$  so that we can write the solution approximation as

$$\mathbf{v}(x) = \mathbf{P}\mathbf{k}(x) \quad (11)$$

and perform a subspace projection of eq. 10, in accordance to classical methods for over-determined systems [14]. This leads to the definition of the following projected matrices

$$\mathbf{E}^\pi = \mathbf{P}^T \mathbf{E} \mathbf{P}, \quad \mathbf{C}^\pi = \mathbf{P}^T \mathbf{C} \mathbf{P}, \quad \mathbf{M}^\pi = \mathbf{P}^T \mathbf{M} \mathbf{P} \quad (12)$$

So the virtual internal work finally reads

$$\delta\mathcal{L}_i^\pi = \int_0^L \delta \begin{bmatrix} \mathbf{k} \\ \mathbf{k}' \end{bmatrix}^T \begin{bmatrix} \mathbf{E}^\pi & \mathbf{C}^\pi \\ \mathbf{C}^{\pi T} & \mathbf{M}^\pi \end{bmatrix} \begin{bmatrix} \mathbf{k} \\ \mathbf{k}' \end{bmatrix} dx \quad (13)$$

This expression is independent from the specific choice of the basis functions. Analogously, the projection of the forcing terms can be defined

$$\mathbf{F}_\Omega^\pi = \mathbf{P}^T \mathbf{F}_\Omega, \quad \mathbf{F}_{\partial\mathcal{A}}^\pi = \mathbf{P}^T \mathbf{F}_{\partial\mathcal{A}}, \quad \mathbf{F}_L^\pi = \mathbf{P}^T \mathbf{F}_L \quad (14)$$

So that the projection of the virtual external work is expressed as

$$\delta\mathcal{L}_e^\pi = \int_0^L \delta\mathbf{k}^T (\mathbf{F}_\Omega^\pi + \mathbf{F}_{\partial\mathcal{A}}^\pi) dx + \delta\mathbf{k}^T(L) \mathbf{F}_L^\pi \quad (15)$$

This projection-based approach is common in many model reduction problems [15, 16]. In this work, we don't look for a mathematical optimality criterion for the definition of matrix  $\mathbf{P}$ , since this often requires some knowledge of the full-system solution  $\mathbf{v}(x)$ , like in Proper Orthogonal Decomposition (POD) approaches [16]. Instead, we compare different a priori choices of matrix  $\mathbf{P}$  based on an assessment of their computational cost and convergence trends, thus avoiding full-system computations.

A fully discrete formulation is obtained once we introduce a set of nodal  $\mathbb{P}_1$  basis functions along the  $x$ -axis, so that the unknown is discretized as  $\mathbf{k}(x) = \boldsymbol{\Theta}(x)\mathbf{h}$ . This leads to the definition of the linear system matrix  $\mathbf{L}$  and forcing  $\mathbf{b}$

$$\begin{aligned} \mathbf{L} &\triangleq \int_0^L \left( \boldsymbol{\Theta}^T \mathbf{E}^\pi \boldsymbol{\Theta} + \boldsymbol{\Theta}^T \mathbf{C}^\pi \frac{d\boldsymbol{\Theta}}{dx} + \frac{d\boldsymbol{\Theta}^T}{dx} \mathbf{C}^{\pi T} \boldsymbol{\Theta} + \frac{d\boldsymbol{\Theta}^T}{dx} \mathbf{M}^\pi \frac{d\boldsymbol{\Theta}}{dx} \right) dx \\ \mathbf{b} &\triangleq \int_0^L \boldsymbol{\Theta}^T (\mathbf{F}_\Omega^\pi + \mathbf{F}_{\partial\mathcal{A}}^\pi) dx + \boldsymbol{\theta}^T(L) \mathbf{F}_L^\pi \end{aligned} \quad (16)$$

so that the final expression of the algebraic linear system to be solved reads  $\mathbf{L}\mathbf{h} = \mathbf{b}$ .

## 4 MODEL PROJECTION APPROACHES

We will compare two alternative choices for matrix  $\mathbf{P}$ . Firstly, the eigenfunctions of the strong form of eq. 10. Lastly, the singular vectors of the cross-section in-plane deformation energy matrix  $\mathbf{E}$ .

### 4.1 Eigenvectors of the Hamiltonian system

A strong form of the semi-discrete variational formulation is obtained by integrating by parts eq. 10, noting that test functions are not allowed to vary on the Dirichlet boundary, and imposing the arbitrariness of variations in the domain  $\delta\mathbf{v}(x)$  and on the Neumann boundary  $\delta\mathbf{v}(L)$ . Defining for convenience matrix  $\mathbf{H} \triangleq \mathbf{C} - \mathbf{C}^T$ , and introducing  $\mathbf{w}(x) \triangleq \mathbf{v}'(x)$ , we can write the corresponding homogeneous system of first order differential equations as

$$\underbrace{\begin{bmatrix} \mathbf{I} & \mathbf{0} \\ \mathbf{0} & \mathbf{M} \end{bmatrix}}_{\mathbf{B}} \frac{d}{dx} \underbrace{\begin{bmatrix} \mathbf{v} \\ \mathbf{w} \end{bmatrix}}_{\mathbf{q}} = \underbrace{\begin{bmatrix} \mathbf{0} & \mathbf{I} \\ \mathbf{E} & \mathbf{H} \end{bmatrix}}_{\mathbf{A}} \underbrace{\begin{bmatrix} \mathbf{v} \\ \mathbf{w} \end{bmatrix}}_{\mathbf{q}} \quad (17)$$

The above system is Hamiltonian, so the spectrum of matrix pair  $(\mathbf{A}, \mathbf{B})$  is symmetric with respect to the imaginary axis. In fact, the same first order system of differential equations can be derived from a Hamiltonian formulation of the semi-discrete problem (eq. 10) [8, 17, 18]. Since the problem is twelve times singular<sup>1</sup>, the eigenvalue computation is ill-conditioned and it is useful to remove the singularity by means of a deflation procedure before performing a numerical eigenvalue computation. The computational procedure used in this work is described in [12].

**Interpretation and assessment of the method.** Eigenvectors related to non-null eigenvalues do show a camber-morphing displacement, making them interesting as basis functions for morphing applications. Eigenvalues real part  $\Re(\lambda_i)$  represents the amplification or damping of each modal shape along the x-axis. This motivates the study of modal truncation as a means for building the projection matrix  $\mathbf{P}$  for morphing applications, since retaining in the model the eigenvectors with the slowest decay rate would allow to analyse the propagation of an imposed shape along the x-axis.

From the computational point of view, some issues when dealing with eigenanalysis of Hamiltonian systems have shown to be relevant in the current application. (a) Eigenvalues of a Hamiltonian system are symmetric with respect to both the real and the imaginary axis, meaning that with a classical eigenvalue solver four new eigenvalues have to be computed before an independent new one is found, making the procedure costly unless specific eigenvalue solvers are employed [20, 21, 22]. (b) No convergence estimates are available for modal truncation of non symmetric systems. (c) The non symmetric Hamiltonian matrix pair of the problem at hand is ill-conditioned, even after mesh scaling has been employed to improve the condition number of matrices  $\mathbf{E}$ ,  $\mathbf{C}$ ,  $\mathbf{M}$ , and after deflation procedures [12] have been employed to desingularize the Hamiltonian matrix pair. (d) Eigenvectors of the Hamiltonian system (eq. 17) exhibit no clear uncoupling of out-of-plane warping displacement from in-plane camber-morphing displacement in most of the eigenfunctions, making it even more difficult to determine the number of eigenvalues which need to be retained in the model in order to have a significant reproduction of a camber morphing behavior.

## 4.2 Eigenvectors of the in-plane deformation energy

Due to the difficulties with the computation of the eigenfunctions of the linear system (eq. 17), we seek an alternative approach for the choice of the basis functions. Matrix  $\mathbf{E}$  is related to a virtual work contribution produced only by in-plane derivatives of the displacement. Recalling here the definition of matrix  $\mathbf{E}$ , together with the cross-section Gram matrix  $\mathbf{W}_S$

$$\mathbf{E} = \int_{\mathcal{A}} (\mathcal{D}_{\xi} \mathbf{N}(\xi))^T \mathbf{D} (\mathcal{D}_{\xi} \mathbf{N}(\xi)) d\mathcal{A}, \quad \mathbf{W}_S = \int_{\mathcal{A}} \mathbf{N}^T(\xi) \mathbf{N}(\xi) d\mathcal{A} \quad (18)$$

<sup>1</sup>As shown in [8], the matrix pair  $(\mathbf{A}, \mathbf{B})$  is defective [19] and it is not diagonalizable, thus a Jordan form decomposition  $\mathbf{A} = \mathbf{B}\mathbf{X}\mathbf{J}\mathbf{X}^{-1}$  is sought [19]. Jordan blocks are related to null eigenvalues associated to bending (two  $4 \times 4$  blocks), axial tension ( $2 \times 2$ ), and torsion ( $2 \times 2$ ) [8], and they generate classical polynomial de Saint Venant's solutions.

we seek a numerical approximation of the most deformable constant shapes from the solution of the real symmetric eigenvalue problem  $\mathbf{E}\mathbf{v}_i = \sigma_i \mathbf{W}_S \mathbf{v}_i$ ,  $i = 1, \dots, R$  for the first  $R$  lowest-modulus non-null eigenvalues, leading to the definition of a matrix of basis functions  $\mathbf{P}_E \equiv [\mathbf{v}_1, \dots, \mathbf{v}_R] \in \mathbb{R}^{3n_s \times R}$ . This matrix is bordered by the de Saint Venant's solution  $\mathbf{P}_d$  computed in the previous section, to give the complete projection matrix  $\mathbf{P} = [\mathbf{P}_E, \mathbf{P}_d]$ .

**Interpretation and assessment of the method.** Looking for the lowest-modulus non-null eigenvalues of matrix pair  $(\mathbf{E}, \mathbf{W}_S)$  means maximizing the cross-section  $L^2$  norm of the solution while considering orthogonal contributions to the internal energy of a deformed shape which doesn't change along the  $x$ -axis

$$\arg \min_{\mathbf{v}_i} (\mathbf{v}_i^T \mathbf{W}_S \mathbf{v}_i) \quad \text{s.t.} \quad \mathbf{v}_i^T \mathbf{E} \mathbf{v}_i = 1, \quad \mathbf{v}_i \notin \ker(\mathbf{E}) \quad (19)$$

For constant solutions along the beam axis, this approach is equivalent to Proper Orthogonal Decomposition (POD) or Singular Value Decomposition (SVD) [16]. The present approach offers several practical advantages over the previous one. (a) Since the virtual work contribution  $\delta \mathbf{v}^T \mathbf{E} \mathbf{v}$  vanishes for the three rigid translation and for a rotation about the  $x$  axis, matrix  $\mathbf{E}$  is positive semidefinite and has four null eigenvalues [8]. Since  $\mathbf{E}$  is symmetric by construction, it is diagonalizable, its eigenvalues are real and its eigenvectors are orthogonal [14]. (b) Clear convergence estimates are available for system SVD (Schmidt–Eckart–Young–Mirsky theorem [16]) and apply for constant solutions along the  $x$  axis. (c) In practice, this means that it is easier for standard eigenvalue solvers to converge on a large number of eigenpairs (in this work, above 300) and to check numerically the convergence of the model for non-constant solutions along the  $x$  axis. (d) Furthermore, camber-morphing and warping singular vectors are naturally uncoupled, as it will be shown in the next paragraph.

Although out-of-plane variations of the deformed shape will be present in most of morphing applications, it is often desirable to keep it at a minimum. In a design phase, uncoupling out-of-plane from in-plane shape variations allows to design the cross-section material layout in order to maximize the desired in-plane morphing behavior.

**Uncoupling of *in-plane* and *out-of-plane* displacement.** It is now convenient to analyze the energy associated to  $\mathcal{D}_\xi \mathbf{u}$  differential operator before any discretization is introduced. We now split the displacement  $\mathbf{u}$  into out-of-plane warping  $u$  and in-plane (camber-morphing) displacement  $\mathbf{c}$ , and move rows of operator  $\mathcal{D}_\xi$  according to the permutation [1, 4, 5, 2, 3, 6] so to partition it as

$$\mathcal{D}_\xi \mathbf{u} = \begin{bmatrix} 0 & 0 & 0 \\ \partial/\partial y & 0 & 0 \\ \partial/\partial z & 0 & 0 \\ 0 & \partial/\partial y & 0 \\ 0 & 0 & \partial/\partial z \\ 0 & \partial/\partial z & \partial/\partial y \end{bmatrix} \begin{bmatrix} u \\ \mathbf{c} \end{bmatrix} \triangleq \begin{bmatrix} 0 & \mathbf{0}^{1 \times 2} \\ \mathcal{D}_\xi^w & \mathbf{0}^{2 \times 2} \\ \mathbf{0}^{3 \times 1} & \mathcal{D}_\xi^c \end{bmatrix} \begin{bmatrix} u \\ \mathbf{c} \end{bmatrix} \quad (20)$$



Figure 2: FishBAC airfoil materials and mesh.

We introduce the same partitioning of the elasticity matrix  $\mathbf{D}$  (eq. 3) through the application of the same permutation  $[1, 4, 5, 2, 3, 6]$  to its rows and columns

$$\mathbf{D} = \begin{bmatrix} 2\mu + \lambda & 0 & 0 & \lambda & \lambda & 0 \\ 0 & \mu & 0 & 0 & 0 & 0 \\ 0 & 0 & \mu & 0 & 0 & 0 \\ \lambda & 0 & 0 & 2\mu + \lambda & \lambda & 0 \\ \lambda & 0 & 0 & \lambda & 2\mu + \lambda & 0 \\ 0 & 0 & 0 & 0 & 0 & \mu \end{bmatrix} = \begin{bmatrix} \mathbf{D}_{00} & \mathbf{0}^{1 \times 2} & \mathbf{D}_{0w} \\ \mathbf{0}^{2 \times 1} & \mathbf{D}_{ww} & \mathbf{0}^{2 \times 3} \\ \mathbf{D}_{0w}^T & \mathbf{0}^{3 \times 2} & \mathbf{D}_{cc} \end{bmatrix} \quad (21)$$

Inserting this partitioning into the expression for the virtual work contribution  $\delta\mathcal{L}_{\mathbf{E}} = \int_{\mathcal{A}} (\mathcal{D}_{\xi} \delta \mathbf{u})^T \mathbf{D} \mathcal{D}_{\xi} \mathbf{u} \, d\mathcal{A}$  and using the adjoint operators<sup>2</sup>  $\mathcal{D}_{\xi}^{w\dagger}$  and  $\mathcal{D}_{\xi}^{c\dagger}$ , we get

$$\begin{aligned} \delta\mathcal{L}_{\mathbf{E}}(x) &= \int_{\mathcal{A}} \left( \begin{bmatrix} 0 & \mathbf{0}^{1 \times 2} \\ \mathcal{D}_{\xi}^w & \mathbf{0}^{2 \times 2} \\ \mathbf{0}^{3 \times 1} & \mathcal{D}_{\xi}^c \end{bmatrix} \begin{bmatrix} \delta u \\ \delta \mathbf{c} \end{bmatrix} \right)^T \begin{bmatrix} \mathbf{D}_{00} & \mathbf{0}^{1 \times 2} & \mathbf{D}_{0w} \\ \mathbf{0}^{2 \times 1} & \mathbf{D}_{ww} & \mathbf{0}^{2 \times 3} \\ \mathbf{D}_{0w}^T & \mathbf{0}^{3 \times 2} & \mathbf{D}_{cc} \end{bmatrix} \begin{bmatrix} 0 & \mathbf{0}^{1 \times 2} \\ \mathcal{D}_{\xi}^w & \mathbf{0}^{2 \times 2} \\ \mathbf{0}^{3 \times 1} & \mathcal{D}_{\xi}^c \end{bmatrix} \begin{bmatrix} u \\ \mathbf{c} \end{bmatrix} \, d\mathcal{A} = \\ &= \int_{\mathcal{A}} \begin{bmatrix} \delta u \\ \delta \mathbf{c} \end{bmatrix}^T \begin{bmatrix} \mathcal{D}_{\xi}^{w\dagger} \mathbf{D}_{ww} \mathcal{D}_{\xi}^w & \mathbf{0}^{1 \times 2} \\ \mathbf{0}^{2 \times 1} & \mathcal{D}_{\xi}^{c\dagger} \mathbf{D}_{cc} \mathcal{D}_{\xi}^c \end{bmatrix} \begin{bmatrix} u \\ \mathbf{c} \end{bmatrix} \, d\mathcal{A} \end{aligned} \quad (22)$$

So matrix  $\mathbf{E}$  appears to be the discretization of a differential operator which uncouples out-of-plane from in-plane displacements.

## 5 ANALYSIS OF CAMBER-MORPHING WING SECTIONS

We analyze the FishBAC (*fishbone active camber*) cross-section proposed by Woods and Friswell in [23] for camber-morphing applications, and further studied in successive works ([24, 25, 26, 27, 28] among others). This is a thin-walled cross-section layout built inside a NACA 0012 airfoil. A sketch of the configuration, with materials layout and the mesh used throughout the analysis is given in fig. 2. A unit-dimension aerodynamic chord is used in the simulations.

Several materials layouts are studied; they are summarized in table 1. Different scalings for the elastic modulus of different materials (identified with reference to their color in figure 2) are chosen in order to enhance the camber-morphing capabilities of the airfoil while keeping a good stiffness in the airfoil nose. Configuration *G* has been used

<sup>2</sup>A procedure for the derivation of adjoint differential operators can be found in [14].

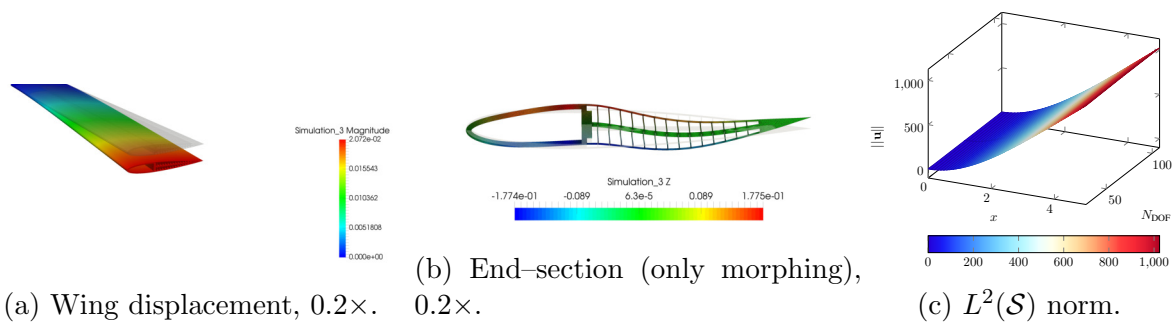


Figure 3: Displacement due to gravity on the FishBAC wing.

for simulations with gravity loads, configuration *A* for imposed shape simulations, and configuration *B* for surface loads.

Table 1: Elastic modulus scaling for each cross-section material (with reference to fig. 2).

|                        | Red | Blue | Yellow | Green |
|------------------------|-----|------|--------|-------|
| Configuration <i>G</i> | 1   | 1    | 1      | 1     |
| Configuration <i>A</i> | 4   | 2    | 1      | 1     |
| Configuration <i>B</i> | 4   | 0.5  | 0.05   | 0.05  |

### 5.1 Three-dimensional simulations with gravity loading

We study a gravity load on the extrusion of length  $L = 5$  of the FishBAC cross-section. This is done by imposing the value  $-\rho g$  in the  $z$ -component of the volume forcing  $\mathbf{f}_\Omega$ . Figure 3 shows the displacement of the wing. A significant camber-morphing behavior is not directly appreciable from fig. 3a, but the modal decomposition allows to filter-out the displacement on the classical deformations  $\mathbf{P}_d$ , so to better visualize the slight morphing deformation which the model is able to capture (fig. 3b). A convergence study for the  $L^2(\mathcal{S})$  norm of the displacement is shown in figure 3c, varying the number of modes retained in the model.

### 5.2 Three-dimensional simulation on imposed modal shapes

From the definition of the eigenvectors of matrix pair  $(\mathbf{E}, \mathbf{W}_S)$ , it is possible to impose a constant morphing solution on a mode  $\mathbf{v}_i$  by simply choosing the forcing terms as  $\mathbf{F}_\Omega = \mathbf{W}_S \mathbf{v}_i$ ,  $\mathbf{F}_L = \mathbf{C}^T \mathbf{v}_i$  and setting an inhomogeneous Dirichlet boundary condition at the root on the desired mode  $\mathbf{v}(0) = \mathbf{v}_i$ . The same could be done for any prescribed solution made of a desired linear combination of eigenvectors.

In order to study the evolution of the morphing shape along the  $x$ -axis, it is more interesting to impose the same forcing while leaving the root boundary conditions homogeneous, i.e. in the undeformed configuration. This is done for eigenvector 8. Results are shown in fig. 4.

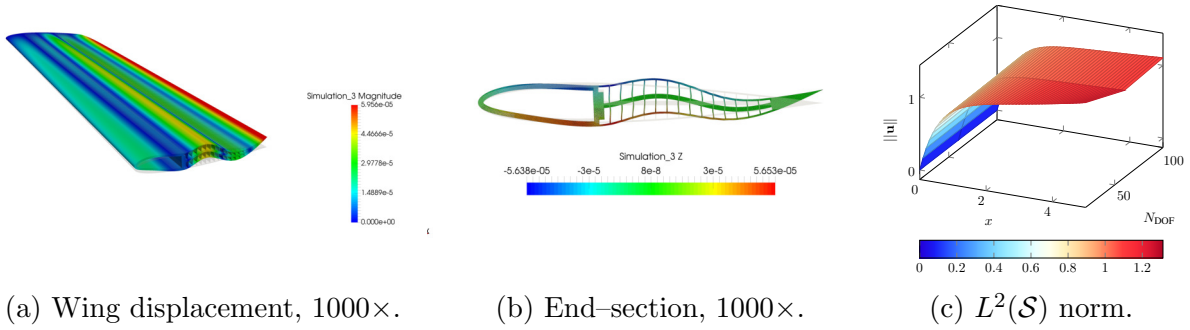


Figure 4: Displacement due to forcing on eigenvector 8 for the FishBAC airfoil.

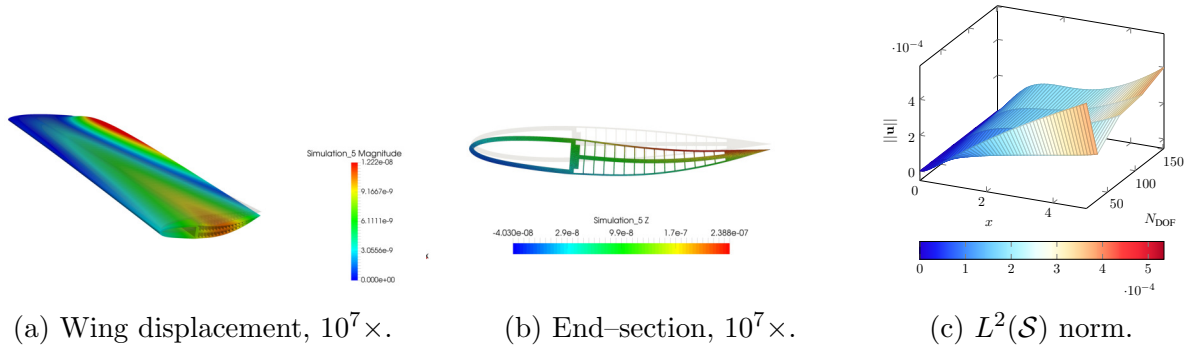


Figure 5: Displacement due to analytical pressure load.

### 5.3 Three-dimensional simulations with analytical pressure loading

A preliminary three-dimensional simulation with surface loading is performed by assigning an analytical pressure distribution on the lateral surface  $\partial\Omega \setminus \{\mathcal{S}_0 \cup \mathcal{S}_L\}$ . We define the coordinate  $\theta(\boldsymbol{\xi})$  and an analytical pressure function  $P(x, \boldsymbol{\xi})$  as

$$\theta(\boldsymbol{\xi}) = \text{sign}(z) \arccos \left( 2 \frac{y - y_0}{y_{\max} - y_{\min}} - 1 \right) \quad (23)$$

$$P(x, \boldsymbol{\xi}) = \frac{1}{L} \sqrt{L^2 - x^2} (C + A_0 \sin^2 \theta(\boldsymbol{\xi}) + A_1 \sin \theta(\boldsymbol{\xi})) \quad (24)$$

Parameter values  $C = 1$ ,  $A_0 = 0.5$ ,  $A_1 = 0.5$  have been used in the simulations. The rationale is to assign a chordwise pressure distribution composed of a constant part plus a symmetrical contribution ( $\sin^2 \theta$ ) and an asymmetrical one ( $\sin \theta$ ). This chordwise pressure distribution is modulated by an elliptical distribution along the x-axis. Finally, resultants are filtered out to obtain a zero-resultant surface load  $\boldsymbol{\tau}$ .

Three-dimensional and cross-section displacements are compared in fig. 5. The displacement is distributed on various modes whose amplitude do vary along the x-axis. Displacements convergence in the  $L^2(\mathcal{S})$  norm is shown in fig. 5.

## 6 CONCLUSIONS

This work proposes an extension of the generalized beam models formulation introduced in [8] for the analysis of camber-morphing constant cross-section structures. We propose a new approach for a projection-based reduced order model, based on the usage of eigenvectors of the in-plane virtual work matrix, and compare it with the usage of the eigenvectors of the Hamiltonian system [12]. Advantages shown by the present method over the previous one are: (a) Theoretical uncoupling of in-plane from out-of-plane displacement basis functions. (b) Well-conditioning of the symmetrical eigenvalue problem. (c) Convergence is observed in practice by increasing the number of basis functions. Results have been shown for test loadings, such as gravity, an imposed displacement solution and prescribed surface pressure. Further work is underway for a coupled fluid-structure interaction simulation.

## References

- [1] Silvestro Barbarino et al. “A Review of Morphing Aircraft”. In: *Journal of Intelligent Material Systems and Structures* 22.9 (June 2011), pp. 823–877.
- [2] Terrence Weisshaar. “Morphing Aircraft Systems: Historical Perspectives and Future Challenges”. In: *Journal of Aircraft* 50.2 (Mar. 2013), pp. 337–353.
- [3] Farhan Gandhi, Mary Frecker, and Andrew Nissly. “Design Optimization of a Controllable Camber Rotor Airfoil”. In: *AIAA Journal* 46.1 (Jan. 2008), pp. 142–153.
- [4] M. Mistry and F. Gandhi. “Design, fabrication, and benchtop testing of a helicopter rotor blade section with warp-induced spanwise camber variation”. In: *Journal of Intelligent Material Systems and Structures* (Aug. 2014), pp. 1–18.
- [5] Tomohiro Yokozeki, Aya Sugiura, and Yoshiyasu Hirano. “Development of Variable Camber Morphing Airfoil Using Corrugated Structure”. en. In: *Journal of Aircraft* 51.3 (May 2014), pp. 1023–1029.
- [6] D. H. Hodges. *Nonlinear Composite Beam Theory*. American Institute of Aeronautics and Astronautics, 2006.
- [7] V. Giavotto et al. “Anisotropic beam theory and applications”. In: *Computers and Structures* 16 (1983).
- [8] M. Morandini, M. Chierichetti, and P. Mantegazza. “Characteristic behavior of prismatic anisotropic beam via generalized eigenvectors”. In: *International Journal of Solids and Structures* 47 (2010).
- [9] A. Mielke. *Hamiltonian and Lagrangian Flows on Center Manifolds - with Applications to Elliptic Variational Problems*. Springer-Verlag, 1991.
- [10] Cornelius O. Horgan. “Recent Developments Concerning Saint-Venant’s Principle: An Update”. In: *Applied Mechanics Reviews* 42.11 (Nov. 1989), pp. 295–303.
- [11] C. O. Horgan. “Recent Developments Concerning Saint-Venant’s Principle: A Second Update”. In: *Applied Mechanics Reviews* 49.10S (Oct. 1996), S101–S111.
- [12] L Cirrottola, M Morandini, and G Quaranta. “A Generalised Beam Formulation for the Dynamic Analysis of Camber-Morphing Helicopter Blades”. In: *International Forum on Aeroelasticity and Structural Dynamics (IFASD 2015)*. 2015, pp. 1–22.

- [13] Janusz S Przemieniecki. *Theory of matrix structural analysis*. Courier Corporation, 1985.
- [14] C. Lanczos. *Linear Differential Operators*. Martino Publishing, 2012 (Reprint of 1961 edition).
- [15] Sigurd Skogestad and Ian Postlethwaite. *Multivariable feedback control: analysis and design*. Vol. 2. Wiley New York, 2007.
- [16] A.C. Antoulas. *Approximation of Large-Scale Dynamical Systems*. Advances in Design and Control. Society for Industrial and Applied Mathematics, 2009.
- [17] Olivier A. Bauchau and Shilei Han. *Advanced Beam Theory for Multibody Dynamics*. 2013.
- [18] Olivier A. Bauchau and Shilei Han. “Three-Dimensional Beam Theory for Flexible Multibody Dynamics”. In: *Journal of Computational and Nonlinear Dynamics* 9.4 (July 2014).
- [19] G. H. Golub and J. H. Wilkinson. “Ill-conditioned eigensystems and the computation of the Jordan canonical form”. In: *SIAM Review* 18 (1976).
- [20] C. Van Loan. “A symplectic method for approximating all the eigenvalues of a Hamiltonian matrix”. In: *Linear Algebra and its Applications* 61 (1984), pp. 233–251.
- [21] Peter Benner and Heike Faßbender. “An implicitly restarted symplectic Lanczos method for the Hamiltonian eigenvalue problem”. In: *Linear Algebra and its Applications* 263 (1997), pp. 75–111.
- [22] Peter Benner, Volker Mehrmann, and Hongguo Xu. “A numerically stable, structure preserving method for computing the eigenvalues of real Hamiltonian or symplectic pencils”. In: *Numerische Mathematik* 78.3 (1998), pp. 329–358.
- [23] Benjamin King Sutton Woods and Michael I. Friswell. *Preliminary Investigation of a Fishbone Active Camber Concept*. 2012.
- [24] Benjamin KS Woods, James HS Fincham, and Michael I Friswell. “Aerodynamic modelling of the fish bone active camber morphing concept”. In: *Proceedings of the RAeS Applied Aerodynamics Conference, Bristol, UK*. Vol. 2224. 2014.
- [25] Benjamin KS Woods, Onur Bilgen, and Michael I Friswell. “Wind tunnel testing of the fish bone active camber morphing concept”. In: *Journal of Intelligent Material Systems and Structures* 25.7 (Feb. 2014), pp. 772–785.
- [26] Benjamin K. Woods and Michael I. Friswell. “Structural Characterization of the Fish Bone Active Camber Morphing Airfoil”. In: *AIAA SciTech Forum*. American Institute of Aeronautics and Astronautics, Jan. 2014.
- [27] Benjamin K. S. Woods, Iman Dayyani, and Michael I. Friswell. “Fluid/Structure-Interaction Analysis of the Fish-Bone-Active-Camber Morphing Concept”. In: *Journal of Aircraft* 52.1 (Nov. 2014), pp. 307–319.
- [28] JHS Fincham and MI Friswell. “Aerodynamic optimisation of a camber morphing aerofoil”. In: *Aerospace Science and technology* 43 (2015), pp. 245–255.